

## Scour of a cohesive soil by submerged plane turbulent wall jets

### Affouillement d'un sol cohésif par des jets de paroi turbulents plans immergés

K.A. MAZUREK, *Department of Civil & Environmental Engineering, University of Windsor, Windsor, Ontario, Canada, N9B 3P4*

N. RAJARATNAM and D.C. SEGO, *Department of Civil & Environmental Engineering, University of Alberta, Edmonton, Alberta, Canada T6G 2G7*

#### ABSTRACT

This paper presents the results of a laboratory study undertaken to examine the effect of hydraulic variables on the scour of a cohesive soil produced by submerged plane turbulent wall jets. The velocity and thickness of the jet were varied in tests with one cohesive soil in part to determine if repeatable scour experiments by these jets could be performed in cohesive material. Measurements were taken of the scour hole profiles at the asymptotic or equilibrium state of scour, including the maximum depth of scour, the location of the maximum scour depth, and the length of the scour hole. Dimensional analysis is used to show that the scour hole dimensions at asymptotic state can be expressed as a function of the velocity at the nozzle, the density of the eroding fluid, the nozzle thickness, and the critical shear stress of the soil. The scour hole profiles are shown to scale with the maximum depth of scour and the distance from the nozzle where the scour is half the maximum scour depth. Observations of the growth of the scour holes are also presented.

#### RÉSUMÉ

Cet article présente les résultats d'une étude de laboratoire entreprise pour examiner l'effet des variables hydrauliques sur l'affouillement d'un sol cohésif produit par les jets de paroi turbulents plans immergés. Dans les essais, on a fait varier la vitesse et l'épaisseur du jet sur un même sol cohésif en partie pour déterminer si des expériences répétables d'affouillement par ces jets peuvent être exécutées en matériau cohésif. Les profils de cuvette ont été mesurés à l'état asymptotique ou état d'équilibre de l'affouillement; ces mesures comprennent la profondeur maximum atteinte et sa localisation, ainsi que la longueur de l'affouillement. En utilisant l'analyse dimensionnelle, on montre que les dimensions de cuvette à l'état asymptotique peuvent être exprimées en fonction de la vitesse à l'injecteur, de la densité du fluide d'érosion, de l'épaisseur de l'injecteur, et de la contrainte de cisaillement critique du sol. On montre que les profils de cuvettes se mettent à l'échelle avec la profondeur maximum et la distance à l'injecteur là où la profondeur de cuvette est moitié de la profondeur maximum. Des observations de la croissance des cuvettes d'affouillement sont également présentées.

*Keywords:* Scour; erosion; clays; cohesive soils; turbulent jets; wall jets.

#### Introduction

Research into the erosion of cohesive soils has made little progress that can be applied directly to field situations. In Northern Alberta, Canada, much of the soil is glacial or lacustrine clay, and engineers have had difficulty effectively accounting for erosion when designing hydraulic works for the area (Andres, 1985). Study of the problem is complicated by the many factors that affect the erodibility of cohesive material, the natural inhomogeneity of soil, and the fact that the soil is most often eroded by a turbulent flow which itself is complex. Irrespective of the present state of knowledge, there are still bridge piers to be designed for scour, river banks to be protected from erosion, canals to be designed against degradation, and soil losses from fields to be estimated. As well, there is the local scour downstream of hydraulic structures, created by flow in the form of turbulent water jets, which, if excessive, may undermine the stability of these structures. Examples are the scour downstream of vertical

gates, flip bucket spillways, drops, and culverts. Scour downstream of vertical gates and due to hydraulic jumps are both cases of scour by turbulent plane wall jets.

Much work has been done on the study of scour by plane turbulent wall jets of cohesionless materials such as Laursen (1952), Rajaratnam (1981), Ali and Salehi Neyshaboury (1991), Chatterjee *et al.* (1994), and Hogg *et al.* (1997). However, although there have been several studies of the scour of cohesive materials by impinging jets (Moore and Masch, 1962; Mirskhulava *et al.*, 1967; Stein *et al.*, 1993; Mazurek *et al.*, 2001), there have been few studies of scour by wall jets in cohesive soils (Abt and Ruff, 1982; Kuti and Yen, 1976). Abt and Ruff (1982) investigated the scour created at the outlet of a culvert (a horizontal circular wall jet) at prototype scale. They examined the effect of flow rate and culvert diameter on the scour holes produced in one cohesive soil made up of 58% sand, 14% silt, and 28% clay, and 1% organic material. The scour holes were refilled with the soil and recompacted after every experiment so that the



Table 1 Details of experiments.

Experiment	a (mm)	$U_o$ (m/s)	Q (L/s)	R ( $\times 10^3$ )	$\lambda$ (Pa)	$t_d$ (h)	Temp ( $^{\circ}$ C)	$w_p$ (%)	$w_f$ (%)	$S_v$ (kPa)	Notes
2.33/5.2/1	2.33	5.16	1.73	9.97	26,566	96.9	13.1	25.43	27.15	25.3	*
2.33/6.2/1	2.33	6.16	2.07	12.84	37,866	129.0	15.9	26.19	26.94	26.8	*
2.33/7.0/1	2.33	6.98	2.34	10.59	48,736	101.2	4.7	26.28		22.9	*
2.33/7.2/1	2.33	7.17	2.41	10.73	51,444	96.2	4.3	25.73	26.67	28.5	*
2.33/7.2/2	2.33	7.16	2.40	14.48	51,154	122.0	14.7	25.63	27.32	22.9	*
2.33/7.4/1	2.33	7.36	2.47	11.36	54,214	94.4	5.2	26.04			†
2.33/8.0/1	2.33	7.97	2.67	12.22	63,506	163.5	5.0	25.85	27.81	21.1	*
2.33/8.0/2	2.33	8.00	2.69	17.89	63,898	101.0	18.7	26.19	27.48	19.6	*
2.33/8.1/1	2.33	8.13	2.73	12.51	66,173	167.6	5.1	25.90	27.71	22.9	†
2.33/8.1/2	2.33	8.05	2.70	12.26	64,845	122.1	4.8	24.72			†
2.33/8.2/1	2.33	8.18	2.75	12.91	66,948	117.3	6.0	25.99	27.17	22.3	*
2.33/8.5/1	2.33	8.52	2.86	12.79	72,551	169.8	4.4	25.97	27.12	22.9	†
2.33/8.5/2	2.33	8.46	2.84	12.94	71,629	120.7	4.9	26.21	27.87	18.7	*
2.33/8.7/1	2.33	8.67	2.91	13.02	75,208	141.4	4.4	25.72			†
2.33/8.8/1	2.33	8.84	2.97	13.32	78,132	96.6	4.5	26.51	28.01	23.1	†
2.33/9.0/1	2.33	9.03	3.03	16.37	81,443	96.3	10.7	25.93	27.23	21.7	*
2.33/9.3/1	2.33	9.31	3.12	14.08	86,636	120.1	4.6	25.90	26.83	26.7	†
2.33/9.7/1	2.33	9.74	3.27	14.13	94,872	142.9	3.4	25.88	27.76	24.7	†
2.33/9.5/1	2.33	9.50	3.19	15.00	90,330	140.6	6.0		27.53	19.9	*
2.33/9.8/1	2.33	9.85	3.31	18.64	96,926	146.1	12.3	26.02	27.38	21.1	*
2.33/10.2/1	2.33	10.23	3.43	21.29	104,503	126.0	15.8	25.81	27.99	22.9	*
2.33/11.3/1	2.33	11.31	3.80	20.79	127,940	93.0	11.2	26.12	27.20	22.9	*
2.33/11.7/1	2.33	11.66	3.91	21.03	135,824	97.0	10.5	26.35	27.58		*
2.33/12.0/1	2.33	12.03	4.04	24.92	144,588	93.2	15.6	25.88	27.05	23.8	*
2.33/12.3/1	2.33	12.25	4.11	25.50	149,993	100.6	15.8	26.15			*
2.33/12.7/1	2.33	12.72	4.27	27.18	161,518	118.2	16.9	25.96			*
2.33/8.9/1/E	2.33	8.89	2.98	13.98	79,009	72.0	5.9	25.54			*
2.33/10.5/1/E	2.33	10.54	3.54	15.88	111,011	4.0	4.5	26.10	28.06	19.6	*
5.10/4.9/1	5.10	4.86	3.73	17.28	23,628	120.4	7.0	25.35	27.24	21.7	*
5.10/6.0/1	5.10	6.04	4.63	20.38	36,430	149.0	5.2	25.28	27.63	20.8	*
5.10/6.5/1	5.10	6.54	5.02	22.10	42,830	149.2	5.2	25.97	27.32	22.6	*
5.10/7.0/3	5.10	7.03	5.40	23.95	49,475	120.0	5.5	25.30	26.95	22.3	*

Code for Test No.: a (mm)/ $U_o$  (m/s)/No. of tests for given conditions E = evolution test.

† velocity measured using Prandtl tube.

\* velocity measured using nozzle pressure.

and 242 mm long, and to allow the samples to be lifted out of the flume without disturbance. In the final stage of preparation, the soil was cut with a very thin metal wire using the top of the metal band as a guide to ensure all the samples were the same height and to create a level surface. The sample was then carefully set in the flume so that its surface was at the same height as the bottom of the nozzle.

Visual estimates of the length of scour, the maximum depth of scour, and the distance of the maximum scour depth from the nozzle were taken at various intervals during the tests until equilibrium was considered to be reached. Equilibrium is defined as the asymptotic state of scour reached as the scouring rate becomes very small as found by Rajaratnam (1981), Chatterjee *et al.* (1994), and others in the scour of cohesionless materials by plane turbulent wall jets. For these tests, equilibrium was assumed to have occurred when the length of the scour hole

was not observed to change over a period of 24 h. This dimension was used instead of the maximum depth of scour as the maximum scour depth could not be measured without disturbing the sample during the testing process (in preliminary tests it was found that disturbances on the clay surface potentially could cause erosion to occur when it may not otherwise; the maximum depth of scour varied across the sample width so that a good estimate could not be made visually). The tests were run continuously until equilibrium scour was reached with a typical test time of 96 h. After each test, three longitudinal scour hole profiles (profiles parallel to the direction of flow) were measured using a point gauge of a 0.1 mm least count. These sections were at about 50, 75 (centerline), and 100 mm across the width of the block although the exact locations of the sections varied (this was done so that the measurements would give the most representative profiles for a test). After the scour hole profile measurements

were complete, vane shear strength tests were carried out on the sample.

Two tests were also undertaken to examine the growth of the scour hole profiles with time (Tests 2.33/8.9/1/E and 2.33/10.5/1/E). For the selected time intervals of 30 min, 1 h, 2 h, 4 h, 24 h, and at each 24 h interval thereafter, the test was shut down and the sample removed from the flume so that profile measurements along the jet centerline could be taken. Unfortunately, in neither test did the samples reach equilibrium. In the first evolution test, this was because of a sudden, unexplained increase in flow velocity during the test, and in the second the sample eroded completely away.

**Erosion characteristics**

There were three types of erosion observed during these experiments. The first is a flake erosion of the clay surface that occurred at low velocities. The flakes tended to be circular in shape, 2 to 3 mm in diameter, and less than 0.5 mm in thickness. At higher shear stresses, both surface erosion and mass erosion occurred. In the first few hours during the tests, the scour holes formed were smooth and uniform across the width of the sample. There was no obvious removal of chunks of clay, which implies that surface erosion occurred. Later in the tests, small chunks of clay began to be eroded from the samples with dimensions in the order of 2 to 5 mm. Infrequent removal of large chunks (i.e. one or two in a test) with the dimensions in the order of 10 to 40 mm also occurred. Frequent removal of large chunks of clay, with a size of 30 to 40 mm, occurred at the higher velocities tested.

**Results**

Typical equilibrium scour hole profiles are shown in Fig. 2, with a sketch of a scour profile given in Fig. 3, where  $\epsilon_{\infty}$  is the depth of erosion at any location at equilibrium. These typical profiles were measured along the centerline of the jet. The scour across the width of the sample was quite variable and both the scour

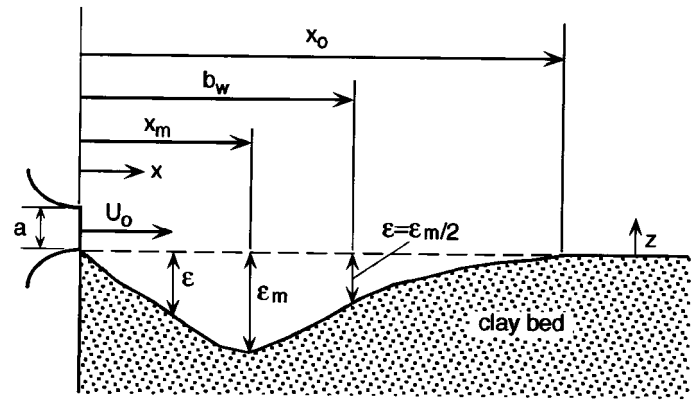


Figure 3 Definition sketch.

hole dimensions and the profile shape could vary across the sample for each test. A scour hole that remained uniform across the sample until equilibrium was reached was the unusual case. This is likely because the samples were primarily eroded by mass erosion, where a chunk of material is eroded from the sample from one location on the sample surface. Mass erosion thus can result in an uneven sample surface, which changes the initially two-dimensional jet flow over the sample to a flow that is much more three dimensional in nature. It is also seen from the profiles in Fig. 2, that there was no deposition of material at the end of the scour holes, unlike that typically observed in the scour of cohesionless materials (Laursen, 1952; Rajaratnam, 1981; Ali and Salehi Neyshaboury, 1991). Abt (1980) observed the formation of a mound at the end of the scour holes in his circular wall jet tests with a cohesive soil, however the soil tested by Abt (1980) was of a much coarser gradation than the soil used in the present experiments.

The growth of the scour holes profiles in the two evolution tests are shown in Fig. 4, with photographic observations of the growth of one of the scour holes shown in Fig. 5. The scour hole dimensions  $\epsilon_m$ ,  $x_m$ , and  $x_0$ , appear to grow in a linear relation with the logarithm of time, as shown in Fig. 6, but as discussed above, do not reach what would be considered an asymptotic or equilibrium state (either by the equilibrium criteria used herein or as shown by the continued growth of the scour holes). It also appears from Fig. 6 that  $x_m$  reaches equilibrium more quickly than either  $\epsilon_m$  or  $x_0$ , which was an observation common to all tests.

**Analysis for the scour holes at equilibrium**

For scour of cohesive material by a plane wall jet, the maximum depth of scour at equilibrium,  $\epsilon_{m\infty}$ , is taken to be a function of

$$\epsilon_{m\infty} = f_1 \{ U_0, a, \rho, \mu, \tau_c \} \tag{1}$$

where  $U_0$  is the velocity at the nozzle,  $a$  is the nozzle thickness,  $\rho$  and  $\mu$  are the density and dynamic viscosity of the eroding fluid, and  $\tau_c$  is the critical shear stress of the soil below which no significant erosion occurs. Dimensional analysis gives

$$\frac{\epsilon_{m\infty}}{a} = f_2 \left\{ \frac{\rho U_0^2}{\tau_c}, \frac{U_0 a}{\nu} \right\} \tag{2}$$

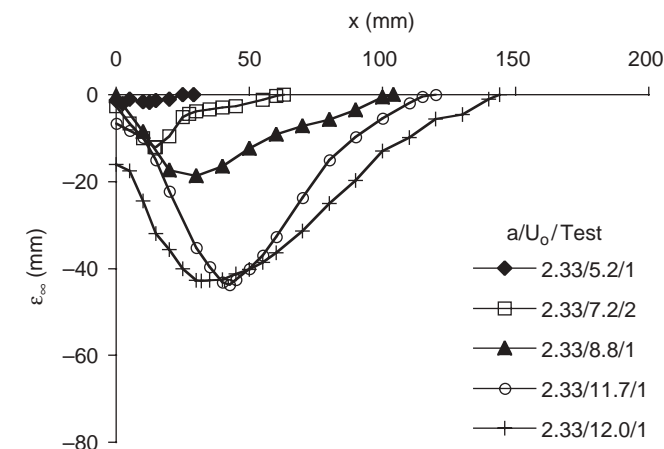


Figure 2 Typical scour hole profiles at equilibrium (measured along jet centerline).

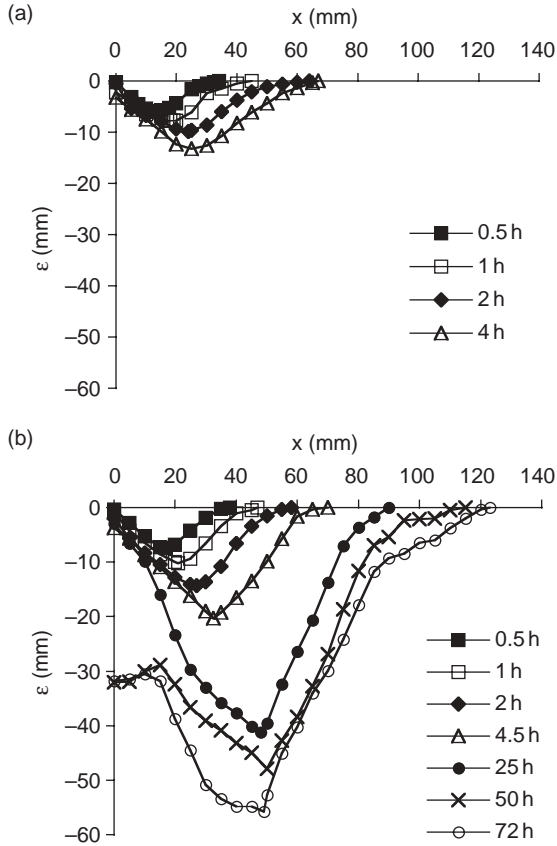


Figure 4 Growth of the scour holes (a) Test No. 2.33/10.5/1/E, (b) Test No. 2.33/8.9/1/E.

The parameter  $U_0 a / \nu$  in Eq. (2) can be recognized as the jet Reynolds number,  $R$ . For  $R$  greater than about  $10^4$ , it appears reasonable to neglect the effect of the Reynolds number on the turbulent jet flow (Rajaratnam, 1976), so that

$$\frac{\varepsilon_{m\infty}}{a} = f_3 \left\{ \frac{\rho U_0^2}{\tau_c} \right\} \quad (3)$$

For convenience, let  $\lambda = \rho U_0^2$ . It can be shown that the ratio  $\lambda / \tau_c$ , is related to ratio  $\tau_{om} / \tau_c$ , where  $\tau_{om}$  is the maximum bed shear stress created by the flow. The bed shear stress  $\tau_{om}$  can be estimated from  $\tau_{om} = c_{fm} (\rho U_0^2 / 2)$ , where  $c_{fm}$  is the coefficient of skin friction at a location very near the nozzle. The coefficient  $c_{fm}$  is known to depend on  $R$ , however this dependence is weak for  $R$  in the range of at least 7,100–56,500 (Myers *et al.*, 1963; Schwarz and Cosart, 1961), and for the purposes herein can be assumed to be constant. Thus

$$\frac{\varepsilon_{m\infty}}{a} = f_4 \left\{ \frac{\tau_{om}}{\tau_c} \right\} \quad (4)$$

The parameter  $\tau_{om} / \tau_c$  is more commonly written in the form of an excess stress  $(\tau_{om} - \tau_c) / \tau_c$ , and following this idea, Eq. (4) becomes

$$\frac{\varepsilon_{m\infty}}{a} = f_5 \left\{ \frac{\tau_{om} - \tau_c}{\tau_c} \right\} \quad (5)$$

Finally, noting that there is a critical value of  $\lambda$ ,  $\lambda_c$ , below which no significant erosion occurs which corresponds to the

critical shear stress of the soil ( $\tau_c = (c_{fm}/2)\lambda_c$ ), Eq. (5) can be equivalently written

$$\frac{\varepsilon_{m\infty}}{a} = f_6 \left\{ \frac{\lambda - \lambda_c}{\lambda_c} \right\} \quad (6)$$

Use of the excess shear stress term in the simpler form  $(\lambda - \lambda_c) / \lambda_c$  of avoids use of empirical information for  $c_{fm}$ , so that the functional form given in Eq. (6) will be used for the present work. Through similar dimensional reasoning, it can be written for the length of the scour hole,  $x_{o\infty}$ , and the distance from the nozzle of the maximum scour depth,  $x_{m\infty}$

$$\frac{x_{o\infty}}{a} = f_7 \left\{ \frac{\lambda - \lambda_c}{\lambda_c} \right\} \quad (7)$$

$$\frac{x_{m\infty}}{a} = f_8 \left\{ \frac{\lambda - \lambda_c}{\lambda_c} \right\} \quad (8)$$

The distances  $x_{m\infty}$  and  $x_{o\infty}$  were in fact measured from the start of the soil surface, which was about 2 mm downstream from the nozzle (the thickness of the metal band that held the sample).

As discussed above, it is expected that the dimensions of the scour hole at equilibrium are related to the parameter  $\lambda = \rho U_0^2$ . Figure 7(a) shows the variation of the average maximum scour depth,  $\bar{\varepsilon}_{m\infty}$ , with  $\lambda$ , while Figs. 7(b–i) show the scour holes that are associated with the points indicated in Fig. 7(a). The maximum scour depth  $\bar{\varepsilon}_{m\infty}$  is the average value of the three measurements taken for each test. From Fig. 7, the critical value for  $\lambda$  can be estimated as  $\lambda_c = 20,000$  Pa. Using a  $c_{fm} = 0.005$ , estimated from Myers *et al.* (1963) and Rajaratnam (1965a,b), this gives a  $\tau_c = 50$  Pa for this soil. This compares favorably with the  $\tau_c = 48$  Pa found in a study of the scour by circular impinging jets that used the same soil as the present tests (Mazurek *et al.*, 2001). The scour hole dimensions can then be related to  $(\lambda - \lambda_c) / \lambda_c$  (Figs. 8–10), with the data being best described by the equations

$$\frac{\bar{\varepsilon}_{m\infty}}{a} = 3.78 \frac{(\lambda - \lambda_c)}{\lambda_c} \quad (9)$$

$$\frac{\bar{x}_{m\infty}}{a} = 3.84 \frac{(\lambda - \lambda_c)}{\lambda_c} \quad (10)$$

$$\frac{\bar{x}_{o\infty}}{a} = 27.0 \left( \frac{\lambda - \lambda_c}{\lambda_c} \right)^{0.58} \quad (11)$$

which gave respective correlation coefficients  $r^2$  of 0.78, 0.64, and 0.82. The data from tests 2.33/8.0/1 and 2.33/8.5/2 (point 3 in Fig. 7(a) and the data point nearest to it) were not included in the correlations for  $\bar{\varepsilon}_{m\infty}$  and  $\bar{x}_{m\infty}$ , as the large values for  $\bar{\varepsilon}_{m\infty}$  and  $\bar{x}_{m\infty}$  were the result of a strongly V-shaped scour hole as compared to the other tests. As well, the two highest values of  $x_o$  in Fig. 10 were not measured but estimated from the scour hole profiles for these tests, as the length of the scour hole reached just beyond the end of the sample.

Observations of the scour hole profiles suggested that there might be several different shapes for the profiles. Based on these profiles shapes, the scour hole profiles classified into four types, with a typical profile for each type given in Fig. 11. The Type 1 profile, shown in Fig. 11(a), is smooth, rounded, deep, and short. The Type 2 profile is shallow and long (Fig. 11(b)). The Type 3

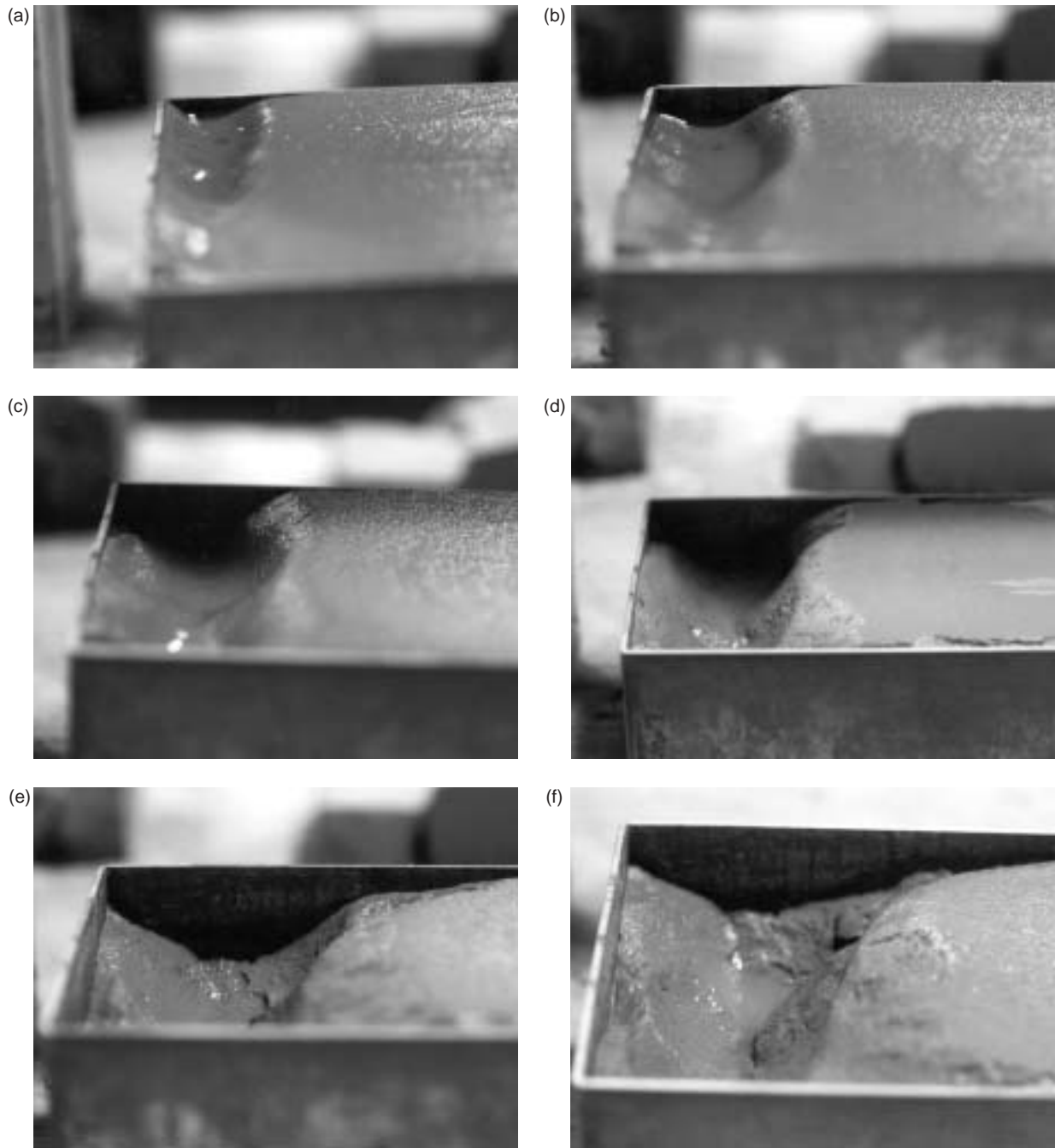


Figure 5 Scour hole growth for Test No. 2.33/8.9/1/E,  $U_o = 8.89$  m/s,  $a = 2.33$  mm after (a) 30 min, (b) 2 h, (c) 4.5 h, (d) 25 h, (e) 50 h, (f) 72 h.

profile is very similar to the Type 1 profile but has a “kink” in the latter half of the scour hole (Fig. 11(b)). The Type 4 profile is also similar to Type 1 but is more V-shaped with an  $x_m$  shifted away from the nozzle (Fig. 11(c)). A few of the profiles could not be classified into any of the four types.

As the scour hole profiles showed that there were different shapes of scour holes, an analysis was carried out as to whether there was an obvious difference in the scour hole geometries between the scour hole types. The different scour hole types did not show any significant differences in  $x_{m\infty}/\varepsilon_{m\infty}$  and no dependence for this ratio on  $(\lambda - \lambda_c)/\lambda_c$ , with  $x_{m\infty}/\varepsilon_{m\infty} \approx 1$ . For  $x_{o\infty}/\varepsilon_{m\infty}$ , the Type 2 scour holes have an average  $x_{o\infty}/\varepsilon_{m\infty} \approx 6$  (which confirms these scour holes are long and shallow) as compared to  $x_{o\infty}/\varepsilon_{m\infty} \approx 3$  for the Type 4 profiles and  $x_{o\infty}/\varepsilon_{m\infty} \approx 4$

for the Type 1 profiles. The Type 3 profiles have large variability in  $x_{o\infty}/\varepsilon_{m\infty}$ . There was less scatter in all of these ratios at high values of  $(\lambda - \lambda_c)/\lambda_c$ . Figures 12–13 show  $\varepsilon_{m\infty}$  and  $x_{m\infty}$  as a function of  $\lambda$  and scour hole type. The Type 2 profiles, although somewhat shallower, do not differ significantly in depth from the other profiles. The Type 2 profiles also tend to have a smaller  $x_m$  (Fig. 13), while no conclusions could be drawn about the  $x_o$ . Since there were no strong tendencies for the scour hole dimensions to depend on the scour hole profile type, it was concluded that using average value for the scour hole dimensions for each test was acceptable for developing predictors of scour.

Several different scales were tried in developing dimensionless equilibrium scour hole profile. The distance from the nozzle,  $b_{w\infty}$ , where  $\varepsilon_{m\infty} = \varepsilon_{m\infty}/2$  on the part of the profile where

$x > x_{m\infty}$  was found to be a suitable scale for the distance from the nozzle and the maximum scour depth works well as the scale for the scour depth. The distances  $x_m$  and  $x_o$  (as in Abt (1980)) were also tried as scales for the distance from the nozzle, but did not work well to collapse the data. The dimensionless profiles for the four different scour hole types are given in Fig. 14(a-d).

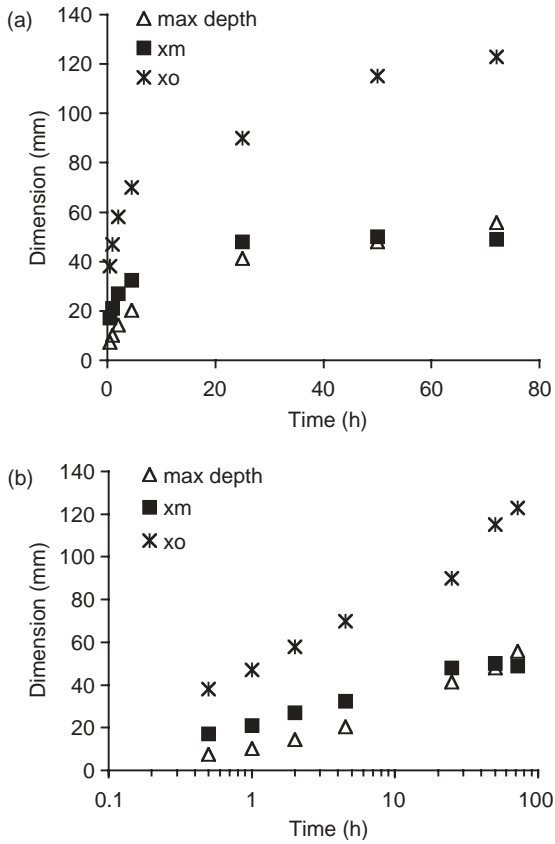


Figure 6 Growth of the scour hole dimensions for Test No. 2.33/8.9/1/E (a) arithmetic scale, (b) semi-log plot.

A fifth power polynomial was found to be a good fit to the Type 1 scour profile (Fig. 14(a)):

$$\frac{\varepsilon_{\infty}}{\varepsilon_{m\infty}} = 1.6 \left( \frac{x}{b_{w\infty}} \right)^5 - 7.5 \left( \frac{x}{b_{w\infty}} \right)^4 + 11.1 \left( \frac{x}{b_{w\infty}} \right)^3 - 4.9 \left( \frac{x}{b_{w\infty}} \right)^2 - 0.22 \left( \frac{x}{b_{w\infty}} \right) - 0.63 \quad (12)$$

This equation departs from the data significantly at  $x/b_{w\infty} > 1.4$  and thus should not be used in this region. The Type 1 profile was included with the other profile types to allow for a comparison of the profile shapes. The Type 3 profile is very similar to the Type 1 profile, but departs from the Type 1 profile for  $x/b_{w\infty} \geq 1$ .

For these dimensionless profiles to be of use, it is then necessary to predict  $b_{w\infty}$ . It was assumed that the relation for  $b_{w\infty}$  should follow the same functional relation as the other scour hole dimensions. Figure 15 shows with relation of  $\bar{b}_{w\infty}$  with  $(\lambda - \lambda_c)/\lambda_c$ . The length scale can then be found using

$$\bar{b}_{w\infty} = 15.14 \left( \frac{\lambda - \lambda_c}{\lambda_c} \right)^{0.56} \quad (13)$$

which gave an  $r^2 = 0.78$ . Here  $\bar{b}_{w\infty}$  is the average of  $b_{w\infty}$  for each test. Although this length scale can be predicted, the scour hole shape that will occur for a given set of conditions as yet cannot be determined.

Analysis of the variability of the scour holes showed that the difference of the maximum scour depth measured along one of the profiles and the average for that test varied from 0.3 to 34.7%. The difference between the largest and smallest values measured for the maximum scour depth for a test varied from 0.5 to 66.9%. For  $x_o$ , both the difference from the average value and the difference between profiles ranged from 0 to 22.5%. The difference from the average for  $x_m$  varied from 0 to 20.0%, while the difference in  $x_m$  between profiles varied from 0 to 42.4%.

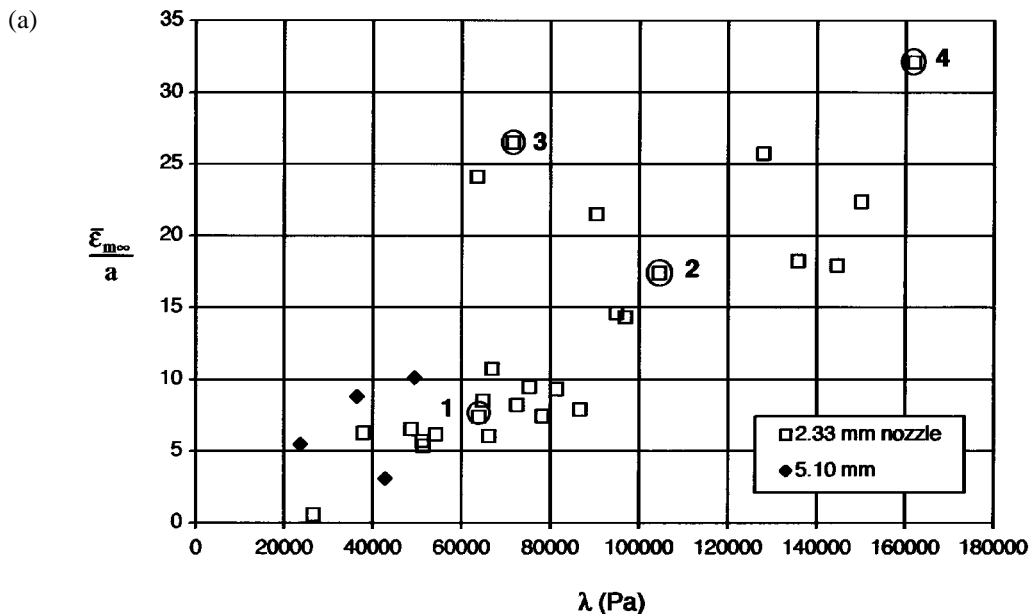


Figure 7

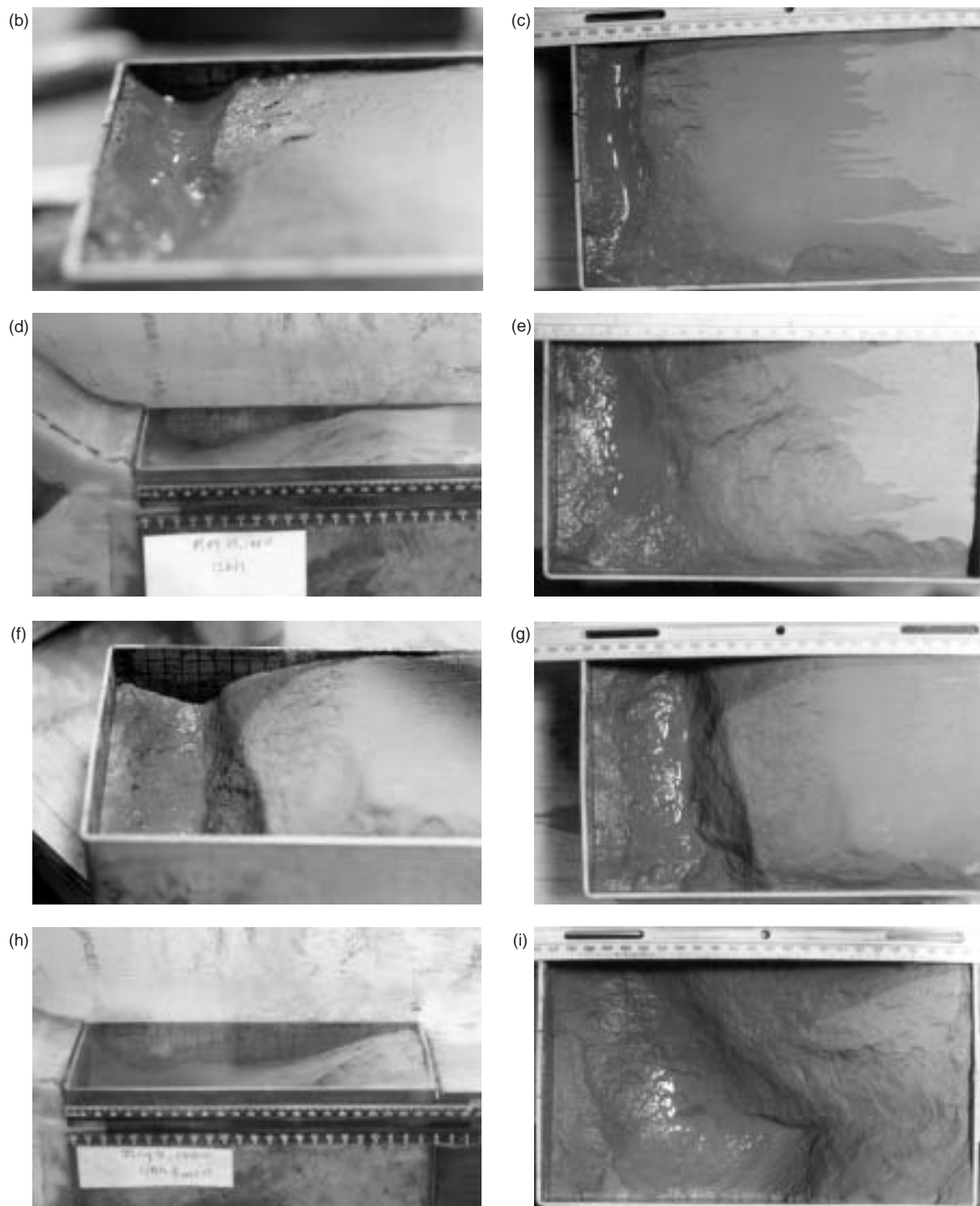


Figure 7 (a) Average maximum scour depth at equilibrium, (b) Point 1 (Test No. 2/33/8/0/2) side view, (c) Point 1 plan view, (d) Point 2 (Test No. 2.33/10.2/1) side view, (e) Point 2 plan view, (f) Point 3 (Test No. 2.33/8/5/2)side view, (g) Point 3 plan view, (h) Point 4 (Test No. 2.33/12.7/1), (i) Point 4 plan view.

### Growth of the scour holes

For the evolution tests, each scour hole profile measured at the different time intervals during each test was made dimensionless using  $\epsilon_m$  and  $b_w$  as scales as for the equilibrium profiles. It was found that the scour hole profiles through each test are similar (Fig. 16). As well, the dimensionless profiles from the two evolution tests fit well with one another and also are very

close to the Type 4 profile developed from the scour hole profiles at equilibrium. Further testing is needed to predict the growth of the scour hole dimensions.

### Discussion and conclusions

For the scour of cohesive material by submerged plane turbulent wall jets, the dimensions of the scour hole created by the jets

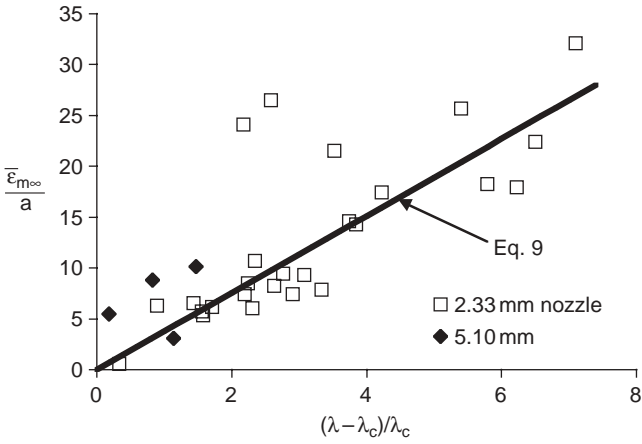


Figure 8 Maximum scour depth at equilibrium.

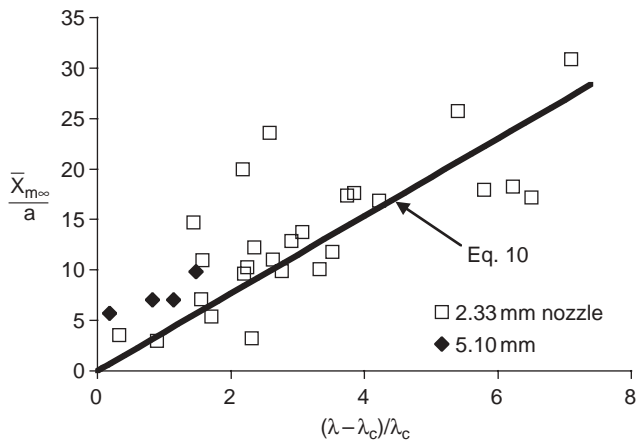


Figure 9 Location of maximum depth of scour.

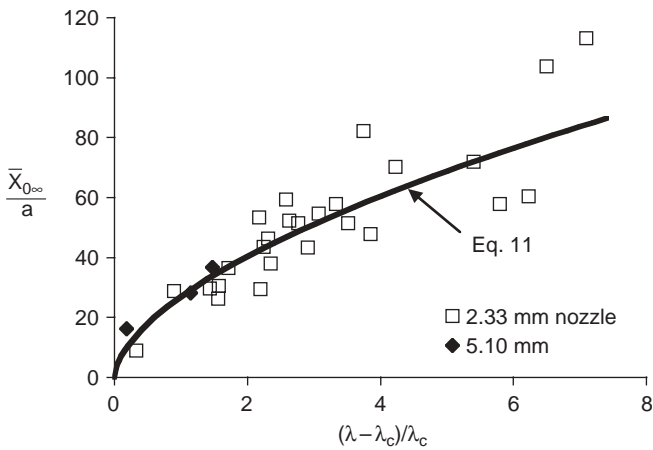


Figure 10 Length of the scour hole at equilibrium.

appear to be related to the velocity and thickness of the jet at the nozzle, the density of the eroding fluid, and the critical shear stress of the soil. The scour hole dimensions appear to scale with the thickness of the jet at the nozzle and can be expressed as a function of the parameter  $(\lambda - \lambda_c)/\lambda_c$ , where  $\lambda = \rho U_0^2$  and  $\lambda_c$  is the value of  $\lambda$  below which no erosion occurs. Predictive equations were developed for the maximum depth of scour, the location of the maximum scour depth, and the length of the scour hole. However, as only one cohesive soil was tested in this work, additional soils must be tested to confirm these relations extend

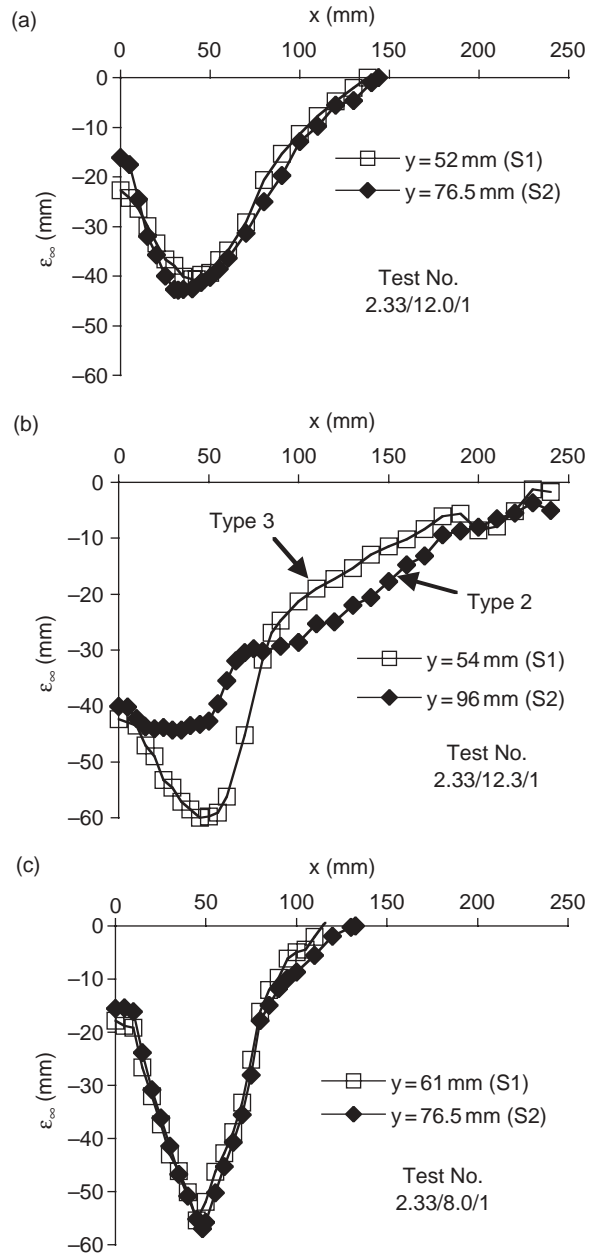


Figure 11 Typical scour hole profiles (a) Type 1 profiles, (b) a Type 2 profile (S2) and a Type 3 profile (S1), and (c) Type 4 profiles.

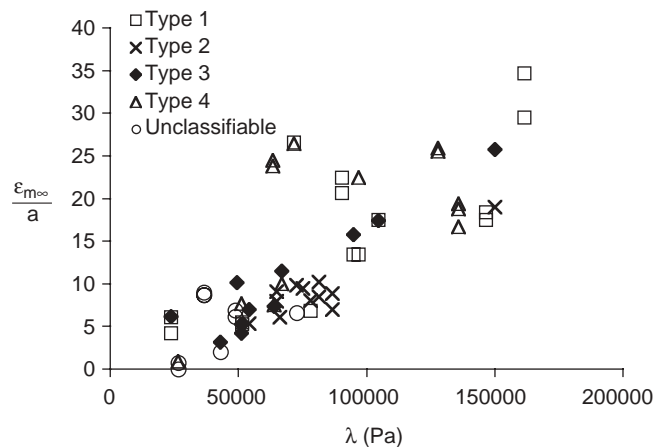


Figure 12 Maximum scour depth at equilibrium sorted by scour hole type.

to other soils. It is unlikely these equations would work well to predict scour in soils that are fissured, highly disturbed by sampling, slaking, layered, or otherwise inhomogeneous.

The scour hole profiles at equilibrium created by the two-dimensional plane wall jet were not two-dimensional, but varied across the width of the sample. This nonuniformity in the scour hole is likely due to the process of scour (although the walls

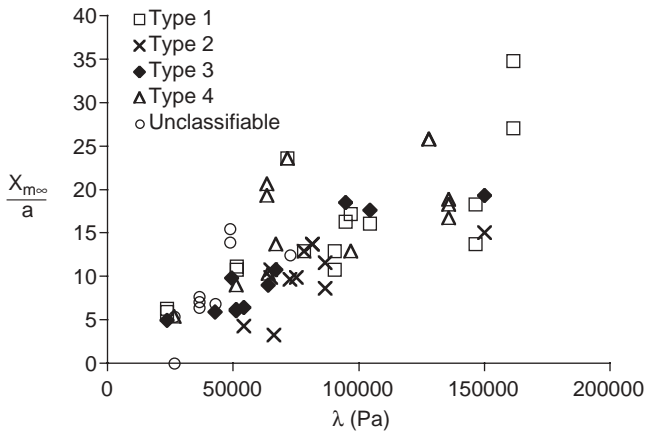


Figure 13 Location of the maximum scour depth at equilibrium sorted by scour hole type.

of the flume and disturbances in the soil created during sample preparation may also have a minor effect). For a soil eroded by mass erosion, an eroded chunk of soil removed from the soil surface, particularly one that is large, results in an uneven soil surface. This disrupts the flow and results in the uneven scour. Not only did  $\epsilon_m$  vary across the width of the sample, the shape of the scour hole profile often varied. The scour hole profiles were sorted by shape and classified into four types. Each type followed its own dimensionless profile. However, the profile that will form under a given set of conditions cannot as yet be predicted.

Observations of the growth of the scour hole profiles along the jet centerline in two tests showed that the dimensionless scour hole profiles measured at each time interval during the test were similar. They also showed the scour hole dimensions grow in a linear relation with the logarithm of time for at least part of the scour hole growth. However, in neither test did the scour holes come to equilibrium. The observations are similar to what has previously been observed in studies of scour by plane wall jets in cohesionless soils (Laursen, 1952; Ali and Salehi Neyshaboury, 1991).

As to whether repeatable experiments can be carried out in the study of scour by plane wall jets, the results show the experiments are repeatable when considering the average dimensions of the scour hole. However, what type of scour hole profile will form

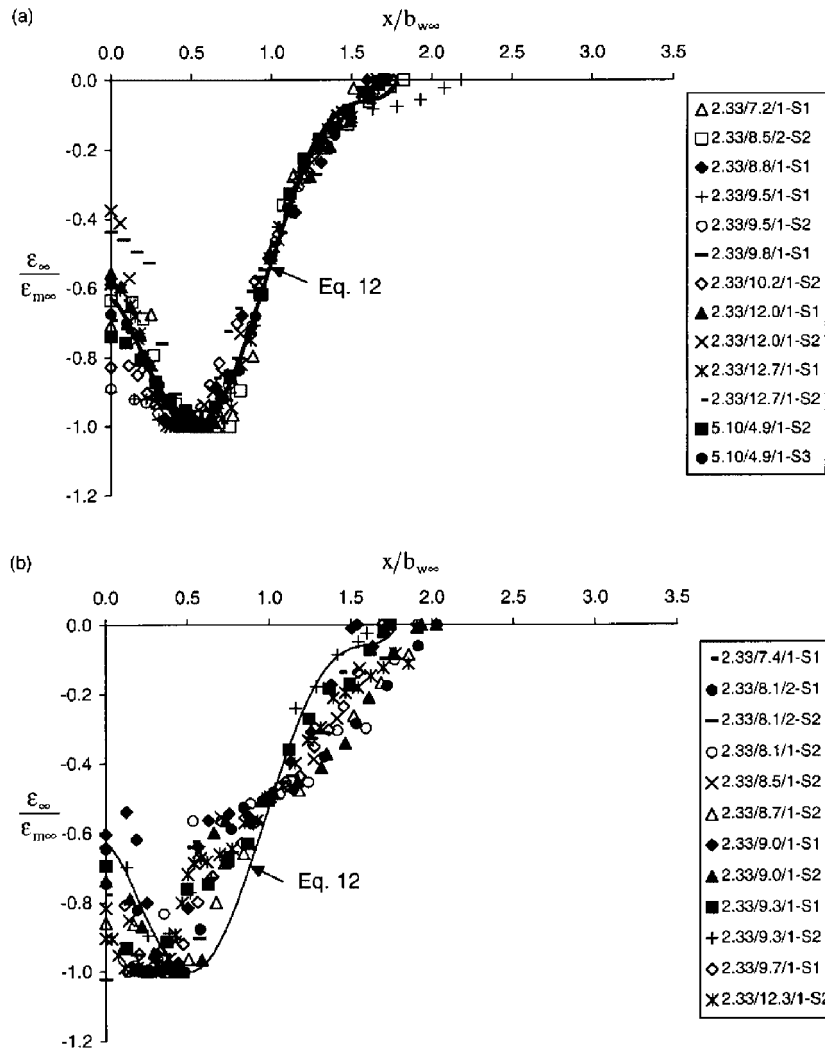


Figure 14

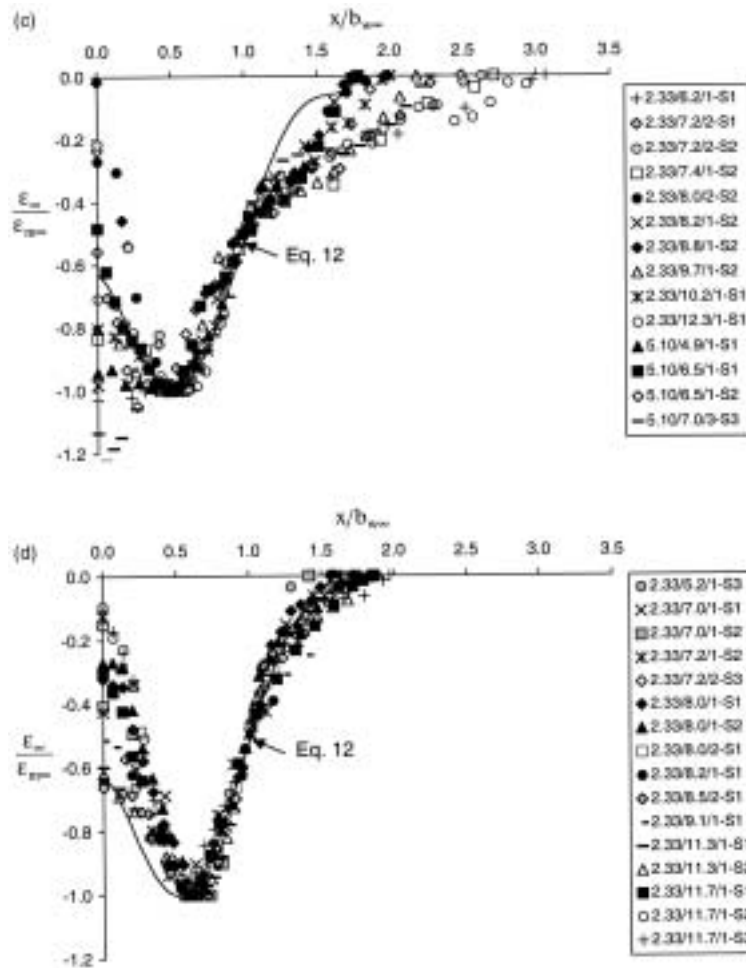


Figure 14 Dimensionless scour hole profiles (a) Type 1, (b) Type 2, (c) Type 3, and (d) Type 4.

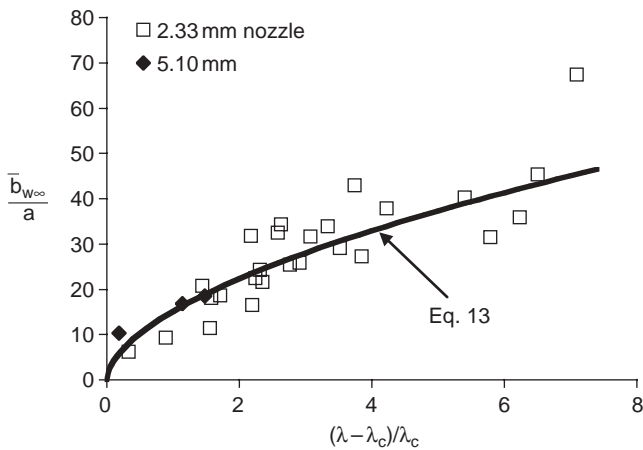


Figure 15 Length scale of scour for equilibrium scour holes.

under given hydraulic conditions is not (as yet) predictable and may not be if that causing the formation of these different profiles is indeed mass erosion. This is because mass erosion currently is not a predictable phenomenon.

**Acknowledgments**

The research described in this paper was performed at the T. Blench Hydraulics Laboratory at the University of Alberta,

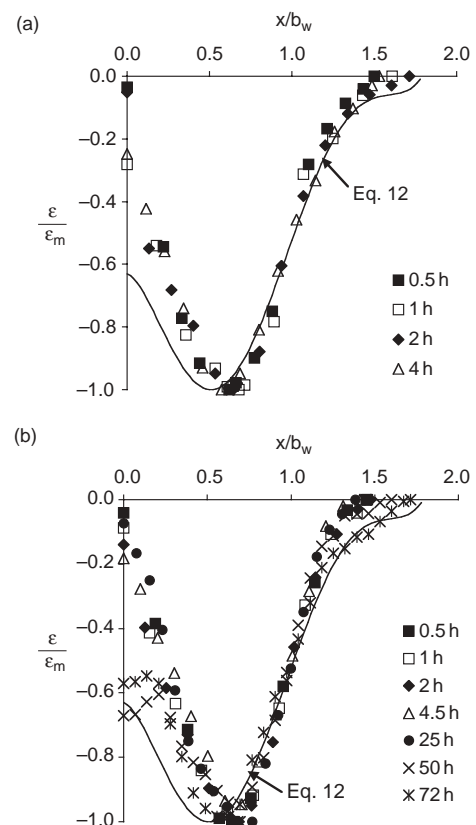


Figure 16 Similarity in the growth of the scour holes (a) Test No. 2.33/10/5/1/E, (b) Test No. 2.33/8.9/1/E.

Edmonton, Alberta, Canada. Support was provided by the Natural Sciences and Engineering Research Council of Canada in the form a scholarship to the first author and a grant to the second. The writers are thankful to P. Fedun for his help in the construction and maintenance of the experimental apparatus and C. Hereygers and S. Gamble for their assistance in determining the properties of the soil.

## Notation

- $a$  = nozzle thickness  
 $b_w$  = distance to half the maximum scour depth ( $x > x_m$ )  
 $b_{w\infty}$  = distance to half the maximum scour depth ( $x > x_m$ ) at equilibrium  
 $\bar{b}_{w\infty}$  = average distance to half the maximum scour depth ( $x > x_m$ ) at equilibrium  
 $c_{fm}$  = skin friction coefficient  
 $r$  = correlation coefficient  
 $R$  = Reynolds number of the jet at the nozzle  
 $U_o$  = velocity at the nozzle  
 $w_p$  = water content of soil sample just prior to start of test  
 $w_f$  = water content of soil sample after test  
 $x$  = distance from the nozzle in the direction of flow  
 $x_m$  = distance from the nozzle of the maximum depth of scour  
 $x_{m\infty}$  = distance from the nozzle of the maximum depth of scour at equilibrium  
 $\bar{x}_{m\infty}$  = average distance from the nozzle of the maximum depth of scour at equilibrium  
 $x_o$  = length of the scour hole  
 $x_{o\infty}$  = length of the scour hole at equilibrium  
 $\bar{x}_{o\infty}$  = average length of the scour hole at equilibrium  
 $y$  = distance across the width of the block as measured from the edge of the sample  
 $\varepsilon_\infty$  = depth of erosion at equilibrium state  
 $\varepsilon_m$  = maximum depth of scour  
 $\varepsilon_{m\infty}$  = maximum depth of scour at equilibrium  
 $\bar{\varepsilon}_{m\infty}$  = average maximum depth of scour at equilibrium  
 $\lambda$  = parameter describing the hydraulic properties of the jet ( $\lambda = \rho U_o^2$ )  
 $\lambda_c$  = critical value of  $\lambda$  below which no significant erosion occurs  
 $\mu$  = dynamic viscosity of the eroding fluid  
 $\rho$  = density of the eroding fluid  
 $\tau_c$  = critical shear stress of the soil  
 $\tau_o$  = shear stress on the clay surface (the wall)

## References

1. ABT, S.R. (1980). Scour at culvert outlets in cohesive bed material, Ph.D. Thesis, Colorado State University, Fort Collins, Colorado, p. 170.
2. ABT, S.R. and RUFF, J.R. (1982). "Estimating Culvert Scour in Cohesive Material", *J. Hydr. Divi. ASCE*, 108(HY1), 25–34.
3. ALI, K.H.M. and SALEHI NEYSHABOURY, A.A. (1991). "Localized Scour Downstream of a Deeply Submerged Horizontal Jet", *Proc. Inst. of Civ. Engrs.*, 91(Mar), 1–18.
4. ANDRES, D. (1985). Hydraulic erodability of cohesive materials, Report No. SWE 83/04, Alberta Research Council, Edmonton, Alberta, Canada, p. 219.
5. CHATTERJEE, S.S., GHOSH, S.N. and CHATTERJEE, M. (1994). "Local Scour due to Submerged Horizontal Jet", *J. Hydr. Engrg. ASCE*, 120(8), 973–992.
6. HOGG, A.J., HUBBERT, H.E. and DADE, W.B. (1997). "Erosion by Planar Turbulent Wall Jets", *J. Fluid Mech.*, 338, 317–340.
7. KUTI, E.G. and YEN, C. (1976). "Scouring of Cohesive Soils", *J. Hydr. Res. IAHR*, 14(3), 195–206.
8. LAURSEN, E.M. (1952). "Observations on the Nature of Scour", *Proc. 5th Hydr. Conference*, State University of Iowa, Iowa City, Iowa, Bulletin 34, 179–197.
9. MAZUREK, K.A. (2001). Scour of clay by jets. Ph.D. thesis, University of Alberta, Edmonton, Alberta, Canada, p. 313.
10. MAZUREK, K.A., RAJARATNAM, N. and SEGO, D.C. (2001). "Scour of Cohesive Soil by Submerged Circular Turbulent Impinging Jets", *J. Hydr. Engrg. ASCE*, 127(7), 1–9.
11. MIRTSKHULAVA, Ts.E., DOLIDZE, I.V. and MAGOMEDOVA, A.V. (1967). "Mechanisms and Computation of Local and General Scour in Non-cohesive, Cohesive Soils, and Rock Beds", *Proc. 12th Congress of the IAHR*, Fort Collins, Colorado, 3, 169–176.
12. MOORE, W.L. and MASCH, F.D. Jr. (1962). "Experiments on the Scour Resistance of Cohesive Sediments", *J. Geophys. Res.*, 67(4), 1437–1449.
13. MYERS, G.E., SCHAUER, J.J. and EUSTIS, R.H. (1963). "The Plane Turbulent Wall Jet Flow Development and Friction Factor", *J. Basic Engrg. Transactions of the ASME*, 85(Mar), 47–53.
14. RAJARATNAM, N. (1965a). "The Hydraulic Jump as a Wall Jet", *J. Hydr. Divi. ASCE*, 91(HY5), 107–132.
15. RAJARATNAM, N. (1965b). "Flow Below a Submerged Sluice Gate as a Wall Jet Problem", *Proc. 2nd Australasian Conference on Hydraulics and Fluid Mechanics*, Auckland, New Zealand, December, Paper No. 2, p. 22.
16. RAJARATNAM, N. (1976). Turbulent jets, Elsevier Scientific Publishing Co., Amsterdam, The Netherlands, p. 304.
17. RAJARATNAM, N. (1981). "Erosion by Plane Turbulent Jets", *J. Hydr. Res. IAHR*, 19(4), 339–358.
18. SCHWARZ, W.H. and COSART, W.P. (1961). "The Two-dimensional Turbulent Wall Jet", *J. Fluid Mech.*, 10, 481–495.
19. STEIN, O.R., JULIEN, P.Y. and ALONSO, C.V. (1993). "Mechanics of Jet Scour Downstream of a Headcut", *J. Hydr. Res. IAHR*, 31(6), 723–738.